Dalton Transactions

PAPER

View Article Online
View Journal | View Issue

Check for updates

Cite this: *Dalton Trans.*, 2024, **53**, 9001

Detection and disaggregation of amyloid fibrils by luminescent amphiphilic platinum(II) complexes†

Zhuoheng Li,[a] Akalanka B. Ekanayake,[a] Anna E. Bartman,[b] Jonathan A. Doorn,[b] Alexei V. Tivanski[a] and F. Christopher Pigge*[a]

Received 25th March 2024,
Accepted 3rd May 2024

DOI: 10.1039/d4dt00882k

rsc.li/dalton

Cyclometallated Pt(II) complexes possessing hydrophobic 2-phenylpyridine (ppy) ligands and hydrophilic acetonylacetone (acac) ligands have been investigated for their ability to detect amyloid fibrils *via* luminescence response. Using hen egg-white lysozyme (HEWL) as a model amyloid protein, Pt(II) complexes featuring benzanilide-substituted ppy ligands and ethylene glycol-functionalized acac ligands demonstrated enhanced luminescence in the presence of HEWL fibrils, whereas Pt(II) complexes lacking complementary hydrophobic/hydrophilic ligand sets displayed little to no emission enhancement. An amphiphilic Pt(II) complex incorporating a bis(ethylene glycol)-derivatized acac ligand was additionally found to trigger restructuring of HEWL fibrils into smaller spherical aggregates. Amphiphilic Pt(II) complexes were generally non-toxic to SH-SY5Y neuroblastoma cells, and several complexes also exhibited enhanced luminescence in the presence of $A\beta_{42}$ fibrils associated with Alzheimer's disease. This study demonstrates that easily prepared and robust (ppy)Pt^{II}(acac) complexes show promising reactivity toward amyloid fibrils and represent attractive molecular scaffolds for design of small-molecule probes targeting amyloid assemblies.

Introduction

Luminescent transition metal complexes are uniquely suited for applications in bioimaging and as biochemical probes.[1–4] Bioprobes incorporating d^6 and d^8 metal complexes of Re, Ru, and Pt possess photophysical properties that offer particularly distinct advantages over purely organic fluorophores.[5,6] For example, these complexes often display long-lived emission through triplet metal–ligand charge transfer (^{3}MLCT) excited states that can be tuned to longer or shorter wavelength as a function of ancillary ligands. Additionally, the physical properties of heteroleptic complexes (*e.g.*, biocompatibility, solubility) can be readily modified by employing appropriately functionalized ligands without adversely affecting desirable photophysical properties. Square planar d^8 Pt(II) complexes possess several other attractive characteristics that render their use in biological applications especially appealing.[7] Depending on the coordinated ligands, emission from planar Pt(II) complexes can reflect mixing of ligand-centered and metal-centered charge transfer transitions to produce long emission lifetimes with large Stokes shifts. Additionally, the square planar geometry leaves axial positions on the Pt(II) centers available for intermolecular interactions, such as with solvent or, upon stacking, with other Pt(II) centers.[8] In turn, Pt–Pt interactions can give rise to significantly red-shifted metal–metal–ligand charge transfer emission (MMLCT). Many Pt(II) complexes, especially cyclometallated complexes (*e.g.*, 2-phenylpyridine Pt complexes) are easily prepared, robust, and display excellent photostability.

Amyloid oligomers and fibrils are formed from self-assembly of misfolded or denatured proteins and polypeptides. Scores of amyloidogenic proteins have been identified, and, despite differences in primary sequence, all amyloid assemblies exhibit similar topological features.[9] Mature amyloid fibrils are characterized by a cross-β-sheet structure in which interstrand β-sheet hydrogen bonding is propagated parallel to the fibril axis. Hydrophobic interactions and other non-covalent attractions mediate association of parallel β-sheets to complete the cross-β-sheet structure and deliver protofibrils. Intertwining of protofibrils then gives rise to mature fibrils. Protofibrils result from dynamic self-assembly of smaller soluble amyloid oligomers. The structure of oligomers is highly variable (dimers, trimers, tetramers, larger structured oligomers, *etc.*) according to the identity and concentration of the amyloid protein monomer.[10–12] Oligomers and fibrils both feature exposed hydrophobic surfaces which provide potential binding sites for hydrophobic probes (such as Thioflavin T)

[a]Department of Chemistry, University of Iowa, Iowa City, Iowa 52242, USA. E-mail: chris-pigge@uiowa.edu
[b]Department of Pharmaceutical Sciences and Experimental Therapeutics, University of Iowa, Iowa City, Iowa 52242, USA

†Electronic supplementary information (ESI) available: All experimental details and additional experimental data. CCDC 2322597–2322599. For ESI and crystallographic data in CIF or other electronic format see DOI: **https://doi.org/10.1039/d4dt00882k**

and, in the case of oligomers, may contribute to biological activity (for example, neurotoxicity of amyloid oligomers assembled from Aβ peptides in Alzheimer's disease).[12,13]

In addition to Alzheimer's disease, amyloid aggregates have been implicated in several other widespread human diseases, including Parkinson's disease and type II diabetes.[14] Consequently, luminescent probes capable of detecting amyloid fibrils/oligomers and influencing the course of amyloid aggregation may offer new approaches for disease diagnosis and therapy.[15,16] The organic dye Thioflavin T (ThT) is the laboratory standard for *ex vivo* detection of mature fibrils, but ThT is not responsive to soluble amyloid oligomers and is not selective for amyloid fibrils in the presence of other proteins and biomolecules. As a result, other organic fluorophores have been investigated as probes for amyloid fibrils,[17–20] and a much smaller subset of compounds has been shown to respond to the presence of soluble amyloid oligomers.[21–32] From these studies common structural features of probe molecules that promote binding to amyloid aggregates have been identified. The most important of these is the presence of extended hydrophobic surfaces, such as found in biaryl, polyaryl, polyaromatic, and stilbene-like fragments, that can interact with exposed hydrophobic sites on amyloid fibrils and oligomers.

Construction of luminescent amyloid probes from transition metal complexes represents an attractive alternative to use of purely organic-derived materials, however this approach has not been extensively explored.[33–35] The metal center in amyloid-sensitive complexes can be utilized not only to impart desirable photophysical properties but also as a synthetic linchpin around which one or more functionalized ligands can be organized in a well-defined geometry. For example, Martí and coworkers have investigated a series of $Ru(bpy)_2^{2+}$ and $Ru(phen)_2^{2+}$ complexes bearing dipyridophenazine (**1**, X = CH) and dipyrazinophenanthroline (**2**, X = N) ligands as probes for Aβ and α-synuclein amyloid aggregates implicated in neurodegenerative diseases (Fig. 1).[36–40] Carlos, *et al.* have examined related $Ru(phen)_2(aminopyridine)_2^{2+}$ complexes for monitoring Aβ and insulin amyloid aggregation,[41–43] while Zhong, *et al.* have reported a tris(heteroleptic) $Ru(dipyridophenazine)^{2+}$ complex that exhibits dual emission for ratiometric monitoring of amyloid aggregation.[44] Several rhenium(I) complexes have been used for luminescence detection of Aβ fibrils. These include a (dipyridophenazine)$Re(CO)_3py^+$ complex reported by Martí (**3**, Fig. 1),[45,46] alkoxy-bridged binuclear Re(vinylpyridine) complexes reported by Rajagopal,[47] and $Re(benzothiazole)_2^+$ polythiophene hybrids prepared and studied in our group (**4**, Fig. 1).[48] Finally, there has been only a single report describing detection of amyloid fibrils using a luminescent Pt(II) complex. Yam and coworkers found that the Pt(bzimpy) complex **5** (Fig. 1) exhibited enhanced long wavelength emission (650 nm) in the presence of amyloid fibrils obtained from bovine insulin.[49] This response was ascribed to binding of the aryl alkynyl ligands to hydrophobic surfaces of the fibril leading to Pt–Pt interactions and long wavelength emission through ^{3}MMLCT excited states.

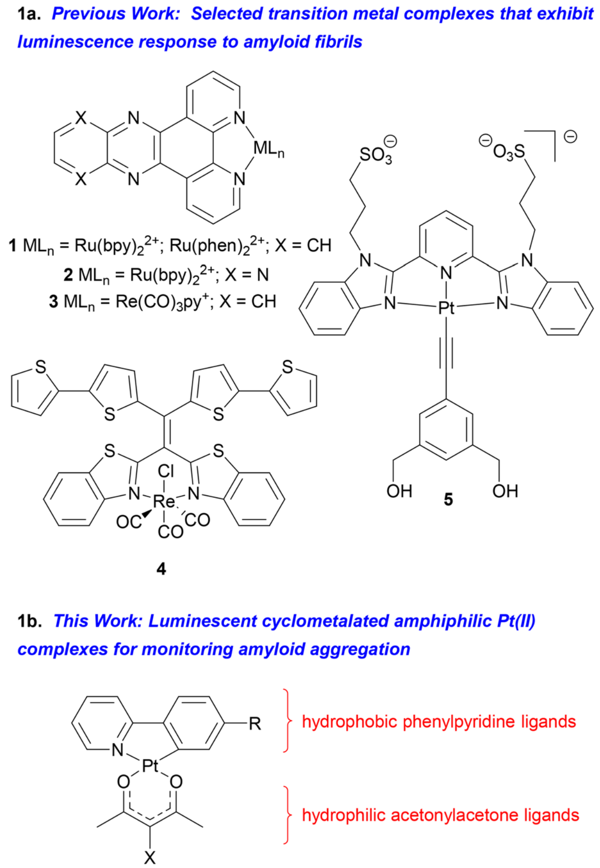

Fig. 1 (a) Examples of luminescent metal complexes used to study amyloid fibrils; (b) outline of complexes examined in this work.

We now report the design and synthesis of new luminescent cyclometalated Pt(II) complexes that show enhanced emission in the presence of amyloid fibrils prepared from hen egg-white lysozyme (HEWL). In particular, complexes displaying amphiphilic properties from a combination of hydrophobic 2-phenylpyridine ligands (ppy) and hydrophilic acetonylacetone (acac) ligands have been investigated. Amphiphilic fluorophores have shown promising activity toward amyloid fibrils,[50–52] and assembling complementary hydrophobic/hydrophilic ligands around square planar Pt(II) metal centers offers attractive opportunities to discover new luminescent amyloid probes. The complex displaying the greatest enhanced emission in the presence of fibrils (**13**) features a benzanilide-substituted ppy ligand and an acac ligand incorporating a bis(diethylene glycol) amide moiety. Complex **13** not only displays 12-fold emission enhancement when treated with HEWL fibrils but also shows the ability to alter the morphology of mature fibrils as determined by atomic force microscopy (AFM) imaging studies.

Results and discussion

Design and synthesis

Cyclometalated Pt(II) acac complexes have been investigated in a number of settings due to their luminescent properties.[53] In the context of probes for amyloid aggregates, we were also attracted to desirable structural properties evident in the parent (ppy)Pt(acac) complex **6** (Scheme 1). Specifically: (1) substituted ppy ligands that provide increased hydrophobic surfaces known to be important for amyloid-binding probes are easily accessible; (2) acac ligands modified with hydrophilic groups are equally easily accessible through straightforward routes; (3) (ppy)Pt(acac) complexes are assembled in highly modular fashion so that ppy and acac ligands can be independently varied; and (4) hydrophobically-driven binding of amphiphilic complexes to amyloid aggregates may result in positioning of hydrophilic acac ligands along the fibril/oligomer periphery, thereby altering the course of further amyloid self-assembly.

A two-step route adapted from established procedures was employed to prepare Pt(II) complexes **6–14** (Scheme 1, see ESI† for experimental details).[54] In the first step, ppy or substituted ppy ligand **L1–L4** was treated with an equimolar amount of K_2PtCl_4 in aqueous 2-ethoxyethanol and heated to 100 °C. The resulting cyclometalated platinum chloride dimers that precipitated from reaction mixtures were then treated with acac or functionalized acac ligand **L5–L8** and base in either 2-ethoxyethanol or 1,4-dioxane at 100 °C. The desired complexes were isolated in the indicated overall yields as air- and moisture-stable materials after purification by flash column chromatography. All new complexes were fully characterized by NMR and mass spectrometry. In addition, single-crystal X-ray structures of complexes **7–9** were successfully obtained (see ESI†).

The hydrophobic ppy ligands examined in this study include a *trans*-stilbene derivative **L2** (**7**, **10**), benzanilide substituted ppy derivative **L3** possessing a 2° amide linkage (**8**, **11–13**), and benzanilide **L4** possessing an *N*-methyl 3° amide linkage (**9**). The stilbene ligand was selected as various stilbene-like molecules are known to exhibit amyloid binding activity.[15,55] The benzanilide substituted ppy ligands incorporate an amide group as a stilbene double bond isostere that also provides additional sites for potential H-bonding interactions with amyloid aggregates.[56,57] Functionalized acac ligands incorporating ethylene glycolate methyl ether **L6** (**10**, **11**),[58] diethylene glycol amide **L7** (**12**), and bis(diethylene glycol) amide **L8** (**13**, **14**) were used to provide the hydrophilic sites of the amphiphilic complexes spatially separated from the hydrophobic ligands *via* the square planar Pt(II) center.

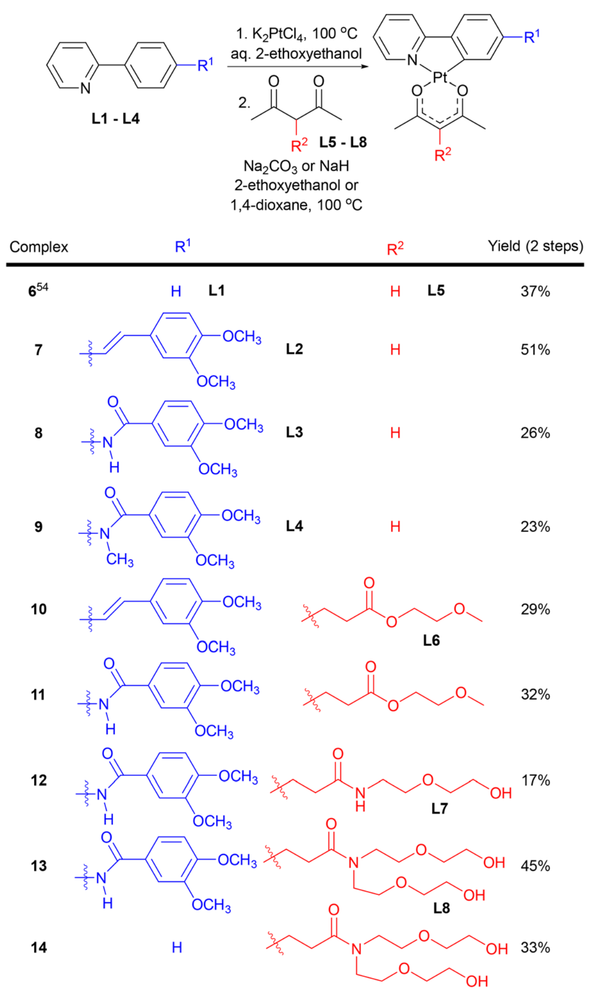

Scheme 1 Synthesis of Pt(II) complexes **6–14**.

Absorption and emission spectra

Absorption spectra for complexes **6–14** were obtained in several solvents of differing polarities and are shown in the ESI (Fig. S1–S9†). In general, all spectra exhibit similar features and UV absorption of individual complexes was largely insensitive to solvent. Higher energy absorptions (<300 nm) are assigned to intraligand transitions, while broad longer wavelength absorptions centered at ~375 nm for the stilbene–ppy hybrid complexes and ~315 nm for the amide-functionalized ppy complexes are attributed to mixed ligand-centered transitions and MLCT. Amide-substituted ppy complexes exhibited a weaker lower energy shoulder that extended to ~425 nm. The identity of the acac ligand does not influence the absorption spectra.

Emission spectra for all complexes were obtained in various solvents using an excitation wavelength of 410 nm. Complexes **7** and **10** bearing the stilbene-like ppy ligand both exhibited broad emission at ~510 nm in CH_2Cl_2 solution that was quenched in aqueous phosphate buffered saline (PBS) (ESI, Fig. S10 and S11†). The emission spectra of the remaining Pt complexes all resemble the emission spectrum of the parent (ppy)Pt(acac) complex **6** (ESI, Fig. S12†) to varying degrees. For example, emission spectra of **8** in organic solvents (Fig. 2a) exhibit structured emission bands similar to those seen for **6** at 500 and 535 nm. In water or PBS solution, however, these structured emission bands are replaced with broad, unstructured, and red-shifted emissions centered at 600 nm, consistent with excimer formation caused by π-stacking of the complex in aqueous solutions. The *N*-methyl analogue **9** displayed similar emission spectra (ESI, Fig. S13†). Excimer emission is observed in aqueous solutions of **6** as well (see ESI, Fig. S12†) and in the solid state.[59]

Fluorescence spectra of **13** in organic solvents also exhibited structured emission bands with λ_{max} ~ 500 nm (Fig. 2b). In

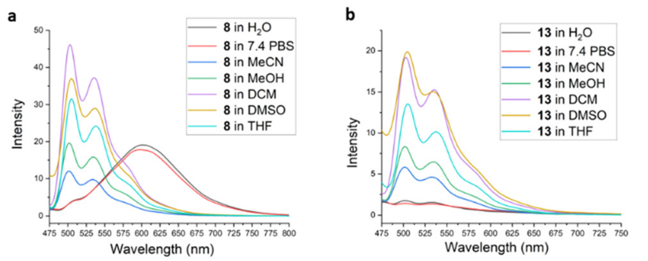

Fig. 2 (a) Emission spectra of **8** in different solvents; (b) emission spectra of **13** in different solvents. [Pt complex] = 10 μM, λ_{ex} = 410 nm. Samples in the indicated solvents also contain 0.5% (v/v) DMSO from Pt complex stock solutions.

contrast with **8**, emission of **13** was quenched in aqueous solutions. This is attributed to the presence of the functionalized hydrophilic acac ligand, rendering **13** more solvated in aqueous environments and impeding hydrophobic stacking interactions. Notably, emission profiles of **11–12** (possessing hydrophilic acac ligands **L6** and **L7**, respectively) and **14** (incorporating an unsubstituted ppy ligand in combination with **L8**) are very similar to **13** (ESI, Fig. S14–S16†).

Dynamic light scattering

To gain insight into Pt(II) complex behaviour in aqueous solutions, dynamic light scattering (DLS) experiments were performed on complexes **8** and **13**. Fig. 3a–c illustrate changes in emission of **8** as a function of H_2O content in aqueous CH_3CN solutions, and Fig. 3d shows the corresponding particle sizes as measured using DLS. Emission at 500 nm was observed to steadily increase with increasing H_2O content up to 60% H_2O/CH_3CN. In aqueous CH_3CN with water fraction >60% the emission at 500 nm decreased concomitantly with increased emission at 600 nm. The average particle size of **8** in 10% aqueous CH_3CN was determined to be ∼320 nm. Particle size decreased to an average size of 110 nm and became more narrowly distributed in solutions containing higher water fraction, up to 60% (corresponding to maximum emission at 500 nm). In 90% H_2O/CH_3CN (corresponding to 600 nm emission), the particle size of **8** was broadly distributed around an average of ∼446 nm.

Amphiphilic complex **13** also exhibited slightly enhanced emission at 500 nm in aqueous CH_3CN up to a H_2O fraction of 70% (Fig. 3e and f) and an average particle size of ∼195 nm (Fig. 3g). At higher water fractions, significantly diminished

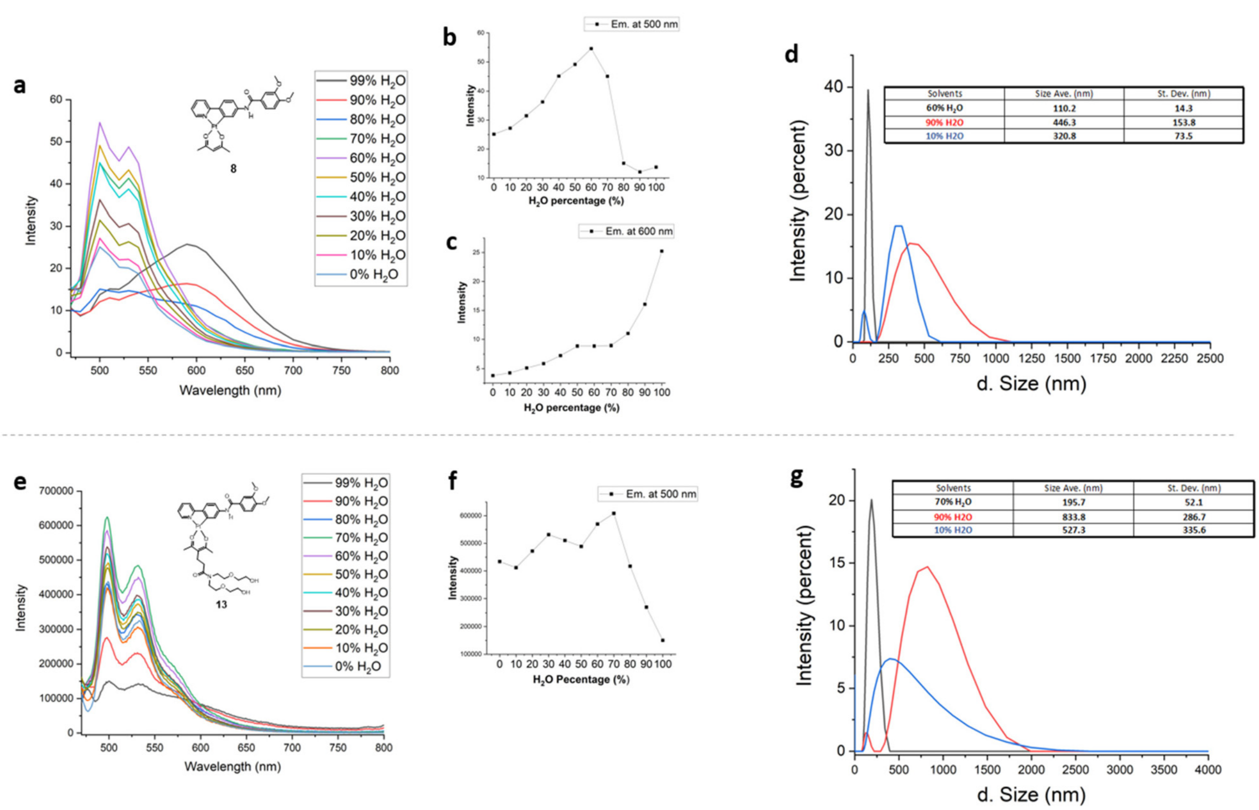

Fig. 3 (a) Emission spectra of **8** (10 μM) in H_2O/CH_3CN mixtures; (b and c) change in emission intensity of **8** (10 μM) as function of H_2O percentage at 500 nm (b) and 600 nm (c), λ_{ex} = 410 nm; (d) DLS measurements of **8** (10 μM) in different H_2O/CH_3CN solutions, black line = 60% H_2O (PDI = 0.650), red line = 90% H_2O (PDI = 0.237), blue line = 10% H_2O (PDI = 0.447); (e) emission spectra of **13** (10 μM) in H_2O/CH_3CN mixtures; (f) change in emission intensity of **13** (10 μM) as function of H_2O percentage at 500 nm, λ_{ex} = 410 nm; (g) DLS measurements of **13** (10 μM) in different H_2O/CH_3CN solutions, black line = 70% H_2O (PDI = 0.287), red line = 90% H_2O (PDI = 0.307), blue line = 10% H_2O (PDI = 0.422).

emission was observed along with increased aggregate particle size (>800 nm in 90% aqueous CH_3CN).

This data suggests that maximum emission of **8** observed in 60% aqueous CH_3CN (λ_{max} 500 nm) arises from relatively small aggregates, around 100 nm in size. At higher H_2O fractions (above 60%), self-assembly of **8** produces larger particles (average size ~ 446 nm) and red-shifted emission tentatively attributed to excimer formation *via* π stacking of the complexes. Similarly, maximum emission of **13** at 500 nm (70% aqueous CH_3CN) is observed to occur from relatively small aggregates with average size of 195 nm. At higher water fraction (>70%) aggregates with larger average particle size are observed but, unlike **8**, these larger aggregates of **13** are essentially non-emissive. We conclude that the functionalized acac ligand in **13** must influence the structure of supramolecular aggregates to impede π stacking and/or Pt–Pt interactions.

Interaction of Pt complexes with HEWL amyloid fibrils

All new Pt complexes were assayed for luminescence response in the presence of amyloid fibrils prepared from hen egg-white lysozyme (HEWL). HEWL is a 129-amino acid protein that forms amyloid fibrils upon denaturation. Moreover, HEWL benefits from wide availability and low cost, making it an attractive model protein for studies of amyloid-binding probes.[60,61] Fibrillization of HEWL was performed under acidic conditions and monitored using a standard ThT fluorescence assay (ESI, Fig. S17†). ThT fluorescence revealed the expected sigmoidal growth curve for fibrillization, consisting of a lag phase for the first ~4 h of incubation followed by rapid fibril growth to attain a stationary phase after ~8 h. Fibril formation under these conditions was confirmed using atomic force microscopy (AFM, *vide infra*).

Aliquots of HEWL incubation solutions taken at different time points were diluted with pH 7.4 PBS solution (to stop fibrillization)[60] in a 96 well plate followed by addition of Pt(II) complex. Luminescence response was then measured using a fluorescence plate reader. In experiments involving the parent (ppy)Pt(acac) complex **6** as well as stilbene-derived ppy complexes **7** and **10**, little to no luminescence enhancement was observed throughout the fibrillization process at the wavelength of maximum emission for each complex (490 nm for **6**, 510 nm for **7** and **10**). In contrast, amide-substituted Pt(acac) complex **8** exhibited a luminescence profile for HEWL fibrillization resembling ThT that resulted in ~6-fold emission enhancement at 510 nm in the presence of fully formed HEWL fibrils. This data is illustrated in Fig. 4a in which emission enhancement (I/I_0) at the λ_{max} for each complex as a function of HEWL incubation time is shown for the four Pt complexes discussed above.

As it appears **8** is capable of binding to HEWL fibrils to produce enhanced emission, luminescence responses of the remaining amide-substituted complexes **9** and **11–13** to HEWL fibrillization were measured and the data is shown in Fig. 4b. Complex **9**, possessing an *N*-methyl amide group on the ppy ligand, and complex **11**, incorporating functionalized acac ligand **L6**, were both inferior to **8** as probes of HEWL fibrillization. Amphiphilic complexes **12** and **13**, however, displayed greater emission enhancement during HEWL fibrillization relative to **8**, an effect attributed to the presence of hydrophilic acac ligands **L7** and **L8**. Moreover, **13** displays enhanced emission at earlier time points of HEWL fibrillization (*i.e.*, after 3 h incubation) compared to other Pt(II) complexes and ThT. This may be indicative of interaction between **13** and pre-fibrillar HEWL aggregates, such as soluble oligomers. Amphiphilicity has been identified as an important characteristic of other amyloid fibril/oligomer probes due to the ability of amphiphilic materials to interact with hydrophobic surfaces of oligomers/fibrils while also engaging with more polar regions of amyloid aggregates.[52] Amphiphilic probes might also shield hydrophobic surfaces of fibrils/oligomers from aqueous solvent, in turn influencing the course of further aggregation and fibril stability. Notably, complex **14** which lacks a functionalized ppy ligand but retains hydrophilic acac **L8** does not show a significant luminescence response to HEWL fibrils (ESI, Fig. S18†), demonstrating the importance of both the substituted ppy and functionalized acac ligands in **13** for mediating fibril interaction.

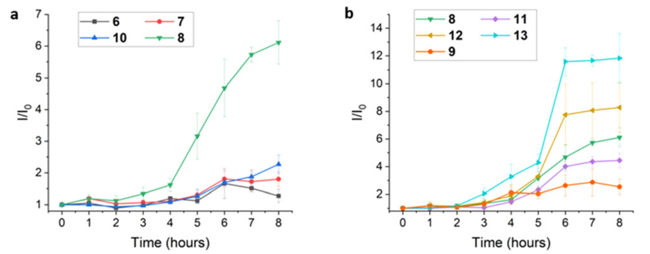

Fig. 4 (a) Plot of emission enhancement (I/I_0) for complexes **6–8** and **10** (20 μM) in the presence of HEWL (10 μM) *versus* HEWL incubation time, λ_{ex} = 410 nm, λ_{em} = 490 nm for **6** and 510 nm for **7–8**, **10**, error bar n = 3; (b) plot of emission enhancement (I/I_0) for complexes **8–9** and **11–13** (20 μM) in the presence of HEWL (10 μM) *versus* HEWL incubation time, λ_{ex} = 410 nm, λ_{em} = 510 nm, error bar n = 3.

Binding assays were performed to quantify the interaction of **8** and **13** with HEWL fibrils. Saturation binding isotherms were generated from luminescence titration experiments in which Pt(II) complex luminescence was measured against a fixed concentration of HEWL fibrils (ESI, Fig. S19 and S20†). The data was analysed by non-linear regression using a one-site binding model to calculate equilibrium dissociation constants (K_d).[48] The calculated K_d for binding of **8** and **13** to HEWL fibrils is 7.9 ± 0.8 μM and 5.5 ± 1.5 μM, respectively. These binding constants reflect the greater luminescence response of **13** toward HEWL fibrils, further highlighting advantages of an amphiphilic probe, although binding is relatively modest in both cases.

Luminescence of **13** (20 μM) in the presence of other biomolecules (10 μM) was briefly examined (ESI, Fig. S21†). The most intense emission response was observed in the presence of HEWL fibrils. Emission to a lesser extent was also noted in the presence of human and bovine serum albumins (HSA, BSA). Little to no luminescence was observed when **13** was combined with HEWL monomers, human immunoglobulin G (IgG), pepsin, and calf thymus DNA (CT DNA).

Atomic force microscopy (AFM) imaging

Successful formation of HEWL fibrils under incubation conditions used in this study was verified by AFM height imaging. After 8 h of incubation under acidic conditions (the time needed for mature fibril formation according to ThT assay described previously), an HEWL stock solution was diluted with pH 7.4 PBS. An aliquot of this solution was used to prepare a sample for AFM imaging which revealed fully formed amyloid fibrils (Fig. 5a). Next, the integrity of HEWL fibrils in the presence of Pt(II) complexes **8** and **13–14** was examined. Aliquots of fully formed HEWL fibril solution were combined with the indicated complexes in pH 7.4 PBS and maintained for 24 h. After this time AFM imaging was performed on each sample and the results are shown in Fig. 5b–d.

Fibrils incubated with **8**, possessing a benzanilide ppy ligand and an unfunctionalized acac ligand, remained essentially unchanged, exhibiting size and shape comparable to control fibrils (Fig. 5b). Likewise, exposure of fibrils to **14** produced no significant changes to fibril size or shape (Fig. 5d). In contrast, AFM revealed that incubation of fibrils for 24 h with amphiphilic complex **13** resulted in dramatic changes to fibril morphology. Rather than typical hair-like structures, aggregates shown in Fig. 5c exhibit sub-micron spherical shapes with average particle height less than half the height of control fibrils and fibrils exposed to complexes **8** and **14**. These results suggest that the combination of ligands in complex **13** not only mediates binding to HEWL fibrils but also promotes the disaggregation and remodelling of fully formed fibrils. Since HEWL fibrillization is performed under strongly acidic conditions, the ability of **13** to inhibit fibril formation was not investigated. However, small molecules capable of disrupting disease-related amyloid aggregates (fibrils and/or oligomers) have been advanced as potential therapeutic agents.[62,63] Future work will examine the ability of **13** and related amphiphilic Pt complexes to affect the fibrillization process of toxic amyloid proteins.

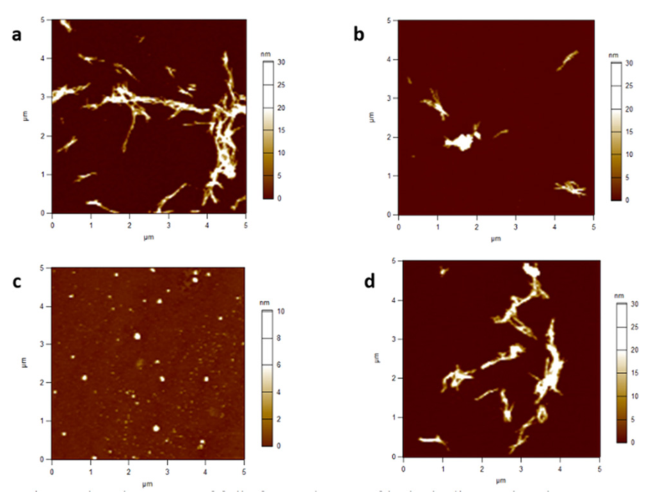

Fig. 5 (a) AFM height image of fully formed HEWL fibrils; (b–d) AFM height images of HEWL fibrils after 24 h exposure to Pt(II) complex **8** (b), Pt(II) complex **13** (c), and Pt(II) complex **14** (d). Scale bars on right indicate particle height.

Detection of Aβ_{42} fibrils

Luminescence response of selected Pt(II) complexes toward amyloid fibrils prepared from disease-relevant peptides was briefly examined. Specifically, samples of fibrils prepared from Aβ_{42}, an amyloidogenic peptide implicated in Alzheimer's disease, were separately treated with platinum complexes **12** and **13**. In each case, ~7-fold luminescence enhancement over Pt(II) complex emission in buffer (PBS) was observed (Fig. 6a). This result indicates that amphiphilic Pt(II) complexes may be suitable for monitoring and/or influencing the aggregation of peptides linked to neurodegeneration.

MTT assay

Experiments were performed to examine the cytotoxicity of selected Pt(II) complexes using MTT cell viability assays. For these experiments, SH-SY5Y neuroblastoma cells were treated with Pt(II) complexes **8** and **11–13** in concentrations ranging from 1 to 100 μM. Untreated cells and cells treated with rotenone (1, 5, and/or 10 μM) were used as positive and negative controls, respectively. Assay results for all four Pt(II) complexes are illustrated in Fig. 7. Only complex **11**, containing a hydrolytically labile ester linkage in the functionalized acac ligand, exhibited any appreciable cytotoxicity in a dose-dependent manner at concentrations of 5 μM and above. The remaining three complexes exhibited essentially no cytotoxicity up to 100 μM. The compatibility of amphiphilic Pt(II) complexes such as **12–13** with SH-SY5Y cells bodes well for use of these and related compounds in *in vivo* settings.

Basis for fibril detection

Several small organic molecules have been found to exhibit enhanced fluorescence in the presence of amyloid fibrils. The

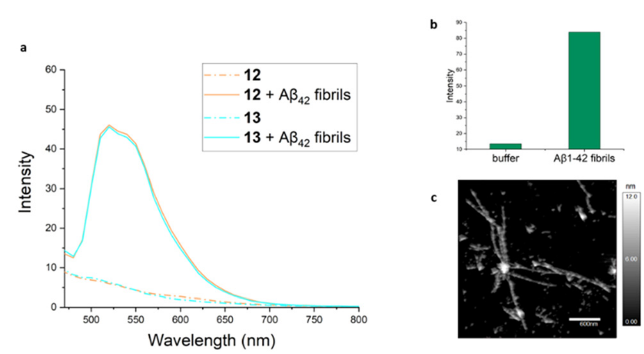

Fig. 6 (a) Luminescence enhancement of Pt(II) complexes **12** (20 μM, light-brown solid line) and **13** (20 μM, cyan solid line) in presence of Aβ_{42} fibrils (10 μM) compared to complex luminescence in the absence of fibrils (dashed lines), λ_{ex} = 410 nm; (b) ThT fluorescence assay of fully formed Aβ_{42} fibrils; (c) AFM image of fully formed Aβ_{42} fibrils.

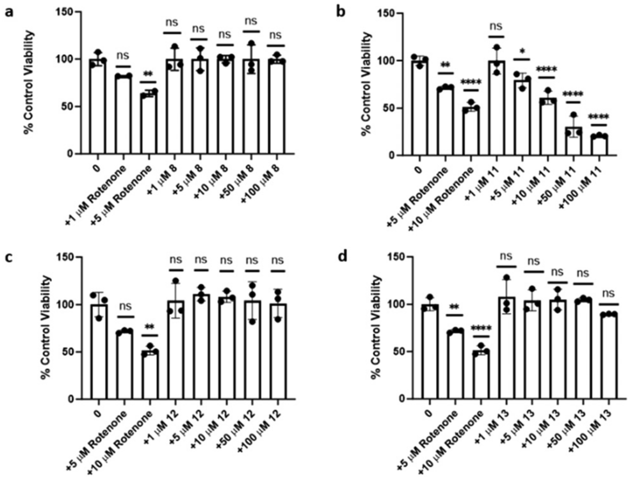

Fig. 7 (a–d) Results of MTT cell viability assays in which SH-SY5Y cells were treated with **8** (a), **11** (b), **12** (c) and **13** (d) at concentrations ranging from 0–100 μM. Data was analyzed using one-way ANOVA with Dunnett's test for multiple comparisons $n = 3$.

basis for fluorescence response is generally ascribed to the ability of non-polar probe molecules to bind hydrophobic fibril surfaces, resulting in restriction of molecular motion and shielding of probe molecules from aqueous solution. A similar rationale is invoked to explain luminescence enhancement of amyloid probes constructed from transition metal complexes (*e.g.*, Fig. 1). The Pt(II) complexes used in this study incorporate hydrophobic cyclometallated 2-phenylpyridine ligands to mediate binding to amyloid surfaces as revealed through enhanced emission. Dynamic light scattering experiments indicate that **8** forms supramolecular aggregates in aqueous solution that exhibit emission at 600 nm. In the presence of HEWL fibrils, however, complex **8** exhibits ~6-fold enhanced emission at shorter wavelength (510 nm) which we ascribe to hydrophobically-driven binding of the Pt(II) complex to exposed non-polar regions of the fibril surface. Thus, introduction of amyloid fibrils to PBS solutions of **8** appears to disrupt 600 nm-emitting Pt(II) complex assemblies in favour of binding to intact fibrils, leading to blue-shifted enhanced emission at 510 nm (Fig. 8a).

Amphiphilic Pt complex **13** binds to HEWL fibrils and promotes fibril disaggregation as detected by AFM imaging (see Fig. 5c). Disruption of amyloid fibril integrity by certain transition metal complexes has been noted in other cases. In some instances, this behaviour is attributed to generation of reactive oxygen species (ROS) that result in degradation of fibril assemblies,[64] while in other instances direct coordination of transition metal centers to amyloid amino acid side chains is believed to be important.[65] Given that (ppy)Pt^{II}(acac) complexes are not especially redox active nor coordinatively labile, neither of these mechanisms appears operative in reactions of fibrils with **13**. Instead, we speculate that the amphiphilicity of **13** is important in driving fibril disaggregation (Fig. 8b). Initial hydrophobically-driven binding of **13** to fibril surfaces may allow interaction between hydrophilic acac ligands and adjacent polar regions of the fibril, leading to breakdown of intertwined protofibrils and formation of the smaller spherical particles detected by AFM. We further speculate that positioning of hydrophilic acac ligands on solvent-exposed surfaces may interfere with the ability of these particles to undergo further aggregation. Notably, while we have used HEWL as a model amyloid protein in this study, topologically related amyloid fibrils from other peptides are believed to play important roles in human diseases such as Alzheimer's and type II diabetes. Utilization of amphiphilic Pt(II) complexes to detect and

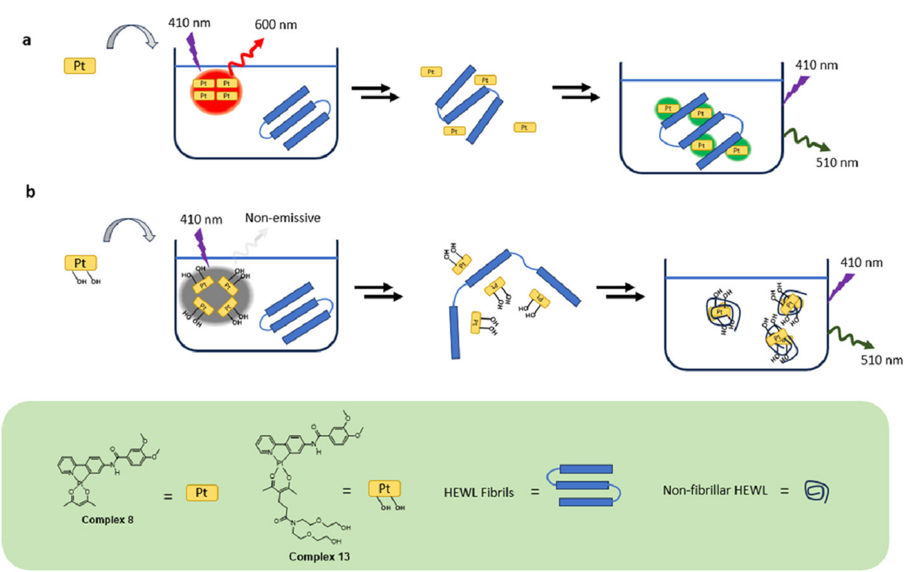

Fig. 8 Schematic depiction of Pt(II) complex interactions with HEWL: (a) interaction of complex **8** with HEWL fibrils; (b) interaction of amphiphilic complex **13** with HEWL fibrils leading to non-fibrillar aggregates.

disrupt disease-relevant protein oligomers and/or fibrils offers new strategies to develop diagnostic or therapeutic organometallic agents targeting amyloid diseases.

Conclusions

This study establishes the ability of amphiphilic cyclometallated Pt(II) acac complexes to detect amyloid fibrils prepared from HEWL *via* enhanced luminescence. In addition, exposure of HEWL fibrils to Pt(II) complex **13**, possessing a hydrophobic benzanilide phenylpyridine ligand and a hydrophilic bis(diethylene glycol) acac ligand, resulted in fibril degradation and formation of smaller spherical protein aggregates as determined by AFM imaging. Other Pt(II) complexes lacking the amphiphilic properties of **13** did not alter the integrity or morphology of HEWL fibrils. The Pt(II) complexes investigated in this work were all easily prepared using a modular synthetic route that should facilitate assembly of additional luminescent Pt(II) complexes bearing complementary ppy and acac chelating ligands spatially separated by the square planar metal center. These complexes offer a convenient organometallic platform from which amyloid-responsive small molecules may be designed for detection and/or alteration of disease-related amyloid oligomers and fibrils. In support of this objective, **13** was shown to exhibit enhanced luminescence in the presence of $A\beta_{42}$ fibrils, an amyloid aggregate associated with Alzheimer's disease. Amphiphilic Pt(II) complexes were further demonstrated to be non-toxic toward SH-SY5Y neuroblastoma cells in MTT cell viability assays. In current work we seek to build on these results and ultimately develop Pt(II) complexes capable of recognizing and modifying small pre-fibrillar oligomers of Aβ peptides implicated as neurotoxic agents in Alzheimer's disease.

Author contributions

Z. L. helped conceive the project, performed experimental work, analyzed the data, and wrote the original draft of the manuscript; Z. L., A. B. E., and A. V. T. conducted AFM imaging studies; A. E. B. and J. A. D. performed MTT assays; F. C. P. conceived the project, supervised the work, and revised the manuscript. All authors reviewed the final manuscript.

Conflicts of interest

There are no conflicts to declare.

Acknowledgements

We thank Prof. Amanda J. Haes and Andrés Mora Mata (University of Iowa) for assistance in performing dynamic light scattering experiments, and Dr. Juan Du and Dr. Joseph Cullen (University of Iowa) for assistance with fluorescence plate reader measurements.

Notes and references

1 L. C.-C. Lee and K. K.-W. Lo, Strategic Design of Luminescent Rhenium(I), Ruthenium(II), and Iridium(III) Complexes as Activity-Based Probes for Bioimaging and Biosensing, *Chem. – Asian J.*, 2022, **17**, e202200840.
2 D.-L. Ma, C. Wu, H. Liu, K.-J. Wu and C.-H. Leung, Luminescence approaches for the rapid detection of disease-related receptor proteins using transition metal-based probes, *J. Mater. Chem. B*, 2020, **8**, 3249–3260.
3 R. Guan, L. Xie, T. W. Rees, L. Ji and H. Chao, Metal complexes for mitochondrial bioimaging, *J. Inorg. Biochem.*, 2020, **204**, 110985.
4 D.-L. Ma, H.-Z. He, K.-H. Leung, D. S.-H. Chan and C.-H. Leung, Bioactive Luminescent Transition-Metal Complexes for Biomedical Applications, *Angew. Chem., Int. Ed.*, 2013, **52**, 7666–7682.
5 L. C.-C. Lee and K. K.-W. Lo, Luminescent and Photofunctional Transition Metal Complexes: From Molecular Design to Diagnostic and Therapeutic Applications, *J. Am. Chem. Soc.*, 2022, **144**, 14420–14440.
6 M. Mauro, A. Aliprandi, D. Septiadi, N. S. Kehr and L. De Cola, When self-assembly meets biology: luminescent platinum complexes for imaging applications, *Chem. Soc. Rev.*, 2014, **43**, 4144–4166.
7 K. Li, G. S. Ming Tong, Q. Wan, G. Cheng, W.-Y. Tong, W.-H. Ang, W.-L. Kwong and C.-M. Che, Highly phosphorescent platinum(II) emitters: photophysics, materials and biological applications, *Chem. Sci.*, 2016, **7**, 1653–1673.
8 V. W.-W. Yam, V. K.-M. Au and S. Y.-L. Leung, Light-Emitting Self-Assembled Materials Based on d^8 and d^{10} Transition Metal Complexes, *Chem. Rev.*, 2015, **115**, 7589–7728.
9 D. S. Eisenberg and M. R. Sawaya, Structural Studies of Amyloid Proteins at the Molecular Level, *Annu. Rev. Biochem.*, 2017, **86**, 69–95.
10 F. Hasecke, T. Miti, C. Perez, J. Barton, D. Schölzel, L. Gremer, C. S. R. Grüning, G. Matthews, G. Meisl, T. P. J. Knowles, D. Willbold, P. Neudecker, H. Heise, G. Ullah, W. Hoyer and M. Muschol, Origin of metastable oligomers and their effects on amyloid fibril self-assembly, *Chem. Sci.*, 2018, **9**, 5937–5948.
11 C. Perez, T. Miti, F. Hasecke, G. Meisl, W. Hoyer, M. Muschol and G. Ullah, Mechanism of Fibril and Soluble Oligomer Formation in Amyloid Beta and Hen Egg White Lysozyme Proteins, *J. Phys. Chem. B*, 2019, **123**, 5678–5689.
12 S. J. C. Lee, E. Nam, H. J. Lee, M. G. Savelieff and M. H. Lim, Towards an understanding of amyloid-β oligomers: characterization, toxicity mechanisms, and inhibitors, *Chem. Soc. Rev.*, 2017, **46**, 310–323.
13 R. Ahmed, M. Akcan, A. Khondker, M. C. Rheinstädter, J. C. Bozelli, R. M. Epand, V. Huynh, R. G. Wylie, S. Boulton, J. Huang, C. P. Verschoor and G. Melacini, Atomic resolution map of the soluble amyloid beta assembly toxic surfaces, *Chem. Sci.*, 2019, **10**, 6072–6082.

14 T. P. J. Knowles, M. Vendruscolo and C. M. Dobson, The amyloid state and its association with protein misfolding diseases, *Nat. Rev. Mol. Cell Biol.*, 2014, **15**, 384–396.
15 K. J. Cao and J. Yang, Translational opportunities for amyloid-targeting fluorophores, *Chem. Commun.*, 2018, **54**, 9107–9118.
16 M. G. Savelieff, G. Nam, J. Kang, H. J. Lee, M. Lee and M. H. Lim, Development of Multifunctional Molecules as Potential Therapeutic Candidates for Alzheimer's Disease, Parkinson's Disease, and Amyotrophic Lateral Sclerosis in the Last Decade, *Chem. Rev.*, 2019, **119**, 1221–1322.
17 M. Staderini, M. A. Martín, M. L. Bolognesi and J. C. Menéndez, Imaging of β-amyloid plaques by near infrared fluorescent tracers: a new frontier for chemical neuroscience, *Chem. Soc. Rev.*, 2015, **44**, 1807–1819.
18 D. Su, W. Diao, J. Li, L. Pan, X. Zhang, X. Wu and W. Mao, Strategic Design of Amyloid-β Species Fluorescent Probes for Alzheimer's Disease, *ACS Chem. Neurosci.*, 2022, **13**, 540–551.
19 F. Tang, K. Wang, X. Liu, X. Zhang, W. Zhou, Z. Mu, T. Zhang, W. Shu, Y. Liu and H. Xiao, Small Molecular Fluorescent Probes for Alzheimer's Disease Associated Active Species, *Chem. – Eur. J.*, 2023, **29**, e202300592.
20 A. Aliyan, N. P. Cook and A. A. Martí, Interrogating Amyloid Aggregates using Fluorescent Probes, *Chem. Rev.*, 2019, **119**, 11819–11856.
21 C. L. Teoh, D. Su, S. Sahu, S.-W. Yun, E. Drummond, F. Prelli, S. Lim, S. Cho, S. Ham, T. Wisniewski and Y.-T. Chang, Chemical Fluorescent Probe for Detection of Aβ Oligomers, *J. Am. Chem. Soc.*, 2015, **137**, 13503–13509.
22 G. Lv, A. Sun, P. Wei, N. Zhang, H. Lan and T. Yi, A spiropyran-based fluorescent probe for the specific detection of β-amyloid peptide oligomers in Alzheimer's disease, *Chem. Commun.*, 2016, **52**, 8865–8868.
23 Y. Li, D. Xu, A. Sun, S.-L. Ho, C.-Y. Poon, H.-N. Chan, O. T. W. Ng, K. K. L. Yung, H. Yan, H.-W. Li and M. S. Wong, Fluoro-substituted cyanine for reliable in vivo labelling of amyloid-β oligomers and neuroprotection against amyloid-β induced toxicity, *Chem. Sci.*, 2017, **8**, 8279–8284.
24 Y. Li, J. Yang, H. Liu, J. Yang, L. Du, H. Feng, Y. Tian, J. Cao and C. Ran, Tuning the stereo-hindrance of a curcumin scaffold for the selective imaging of the soluble forms of amyloid beta species, *Chem. Sci.*, 2017, **8**, 7710–7717.
25 M. Kumar, Y. Hong, D. C. Thorn, H. Ecroyd and J. A. Carver, Monitoring Early-Stage Protein Aggregation by an Aggregation-Induced Emission Fluorogen, *Anal. Chem.*, 2017, **89**, 9322–9329.
26 A. M. Fanni, F. A. Monge, C.-Y. Lin, A. Thapa, K. Bhaskar, D. G. Whitten and E. Y. Chi, High Selectivity and Sensitivity of Oligomeric p-Phenylene Ethynylenes for Detecting Fibrillar and Prefibrillar Amyloid Protein Aggregates, *ACS Chem. Neurosci.*, 2019, **10**, 1813–1825.
27 G. Lv, A. Sun, M. Wang, P. Wei, R. Li and T. Yi, A novel near-infrared fluorescent probe for detection of early-stage Aβ protofibrils in Alzheimer's disease, *Chem. Commun.*, 2020, **56**, 1625–1628.
28 J. Yang, F. Zeng, X. Li, C. Ran, Y. Xu and Y. Li, Highly specific detection of Aβ oligomers in early Alzheimer's disease by a near-infrared fluorescent probe with a "V-shaped" spatial conformation, *Chem. Commun.*, 2020, **56**, 583–586.
29 N. Tonali, V. I. Dodero, J. Kaffy, L. Hericks, S. Ongeri and N. Sewald, Real-Time BODIPY-Binding Assay To Screen Inhibitors of the Early Oligomerization Process of Aβ1–42 Peptide, *ChemBioChem*, 2020, **21**, 1129–1135.
30 L. Sun, H.-J. Cho, S. Sen, A. S. Arango, T. T. Huynh, Y. Huang, N. Bandara, B. E. Rogers, E. Tajkhorshid and L. M. Mirica, Amphiphilic Distyrylbenzene Derivatives as Potential Therapeutic and Imaging Agents for Soluble and Insoluble Amyloid β Aggregates in Alzheimer's Disease, *J. Am. Chem. Soc.*, 2021, **143**, 10462–10476.
31 D. Lee, S. M. Kim, H. Y. Kim and Y. Kim, Fluorescence Chemicals To Detect Insoluble and Soluble Amyloid-β Aggregates, *ACS Chem. Neurosci.*, 2019, **10**, 2647–2657.
32 Y. Wang, J. Chen, F. Gao, M. Hu and X. Wang, Recent developments in the chemical biology of amyloid-β oligomer targeting, *Org. Biomol. Chem.*, 2023, **21**, 4540–4552.
33 B. Jiang and A. A. Martí, Probing Amyloid Nanostructures Using Photoluminescent Metal Complexes, *Eur. J. Inorg. Chem.*, 2021, 4408–4424.
34 E. Babu, J. Bhuvaneswari, K. Rajakumar, V. Sathish and P. Thanasekaran, Non-conventional photoactive transition metal complexes that mediated sensing and inhibition of amyloidogenic aggregates, *Coord. Chem. Rev.*, 2021, **428**, 213612.
35 J. Kwak, J. Woo, S. Park and M. H. Lim, Rational design of photoactivatable metal complexes to target and modulate amyloid-β peptides, *J. Inorg. Biochem.*, 2023, **238**, 112053.
36 N. P. Cook, V. Torres, D. Jain and A. A. Martí, Sensing Amyloid-β Aggregation Using Luminescent Dipyridophenazine Ruthenium(II) Complexes, *J. Am. Chem. Soc.*, 2011, **133**, 11121–11123.
37 N. P. Cook, K. Kilpatrick, L. Segatori and A. A. Martí, Detection of α-Synuclein Amyloidogenic Aggregates in Vitro and in Cells using Light-Switching Dipyridophenazine Ruthenium(II) Complexes, *J. Am. Chem. Soc.*, 2012, **134**, 20776–20782.
38 N. P. Cook, M. Ozbil, C. Katsampes, R. Prabhakar and A. A. Martí, Unraveling the Photoluminescence Response of Light-Switching Ruthenium(II) Complexes Bound to Amyloid-β, *J. Am. Chem. Soc.*, 2013, **135**, 10810–10816.
39 B. Jiang, A. Aliyan, N. P. Cook, A. Augustine, G. Bhak, R. Maldonado, A. D. Smith McWilliams, E. M. Flores, N. Mendez, M. Shahnawaz, F. J. Godoy, J. Montenegro, I. Moreno-Gonzalez and A. A. Martí, Monitoring the Formation of Amyloid Oligomers Using Photoluminescence Anisotropy, *J. Am. Chem. Soc.*, 2019, **141**, 15605–15610.
40 B. Jiang, U. Umezaki, A. Augustine, V. M. Jayasinghe-Arachchige, L. F. Serafim, Z. M. S. He, K. M. Wyss, R. Prabhakar and A. A. Martí, Deconvoluting binding sites in amyloid nanofibrils using time-resolved spectroscopy, *Chem. Sci.*, 2023, **14**, 1072–1081.

41 D. E. S. Silva, M. P. Cali, W. M. Pazin, E. Carlos-Lima, M. T. Salles Trevisan, T. Venâncio, M. Arcisio-Miranda, A. S. Ito and R. M. Carlos, Luminescent Ru(II) Phenanthroline Complexes as a Probe for Real-Time Imaging of Aβ Self-Aggregation and Therapeutic Applications in Alzheimer's Disease, *J. Med. Chem.*, 2016, **59**, 9215–9227.
42 M. P. Cali, L. M. B. Pereira, M. D. Teodoro, T. A. Sellani, E. G. Rodrigues and R. M. Carlos, Comparison of Aβ (1–40, 1–28, 11–22, and 29–40) aggregation processes and inhibition of toxic species generated in early stages of aggregation by a water-soluble ruthenium complex, *J. Inorg. Biochem.*, 2021, **215**, 111314.
43 L. M. B. Pereira, M. P. Cali, R. C. Marchi, W. M. Pazin and R. M. Carlos, Luminescent imaging of insulin amyloid aggregation using a sensitive ruthenium-based probe in the red region, *J. Inorg. Biochem.*, 2021, **224**, 111585.
44 J.-Y. Shao, S.-H. Wu, J. Ma, Z.-L. Gong, T.-G. Sun, Y. Jin, R. Yang, B. Sun and Y.-W. Zhong, Ratiometric detection of amyloid-β aggregation by a dual-emissive tris-heteroleptic ruthenium complex, *Chem. Commun.*, 2020, **56**, 2087–2090.
45 A. Aliyan, B. Kirby, C. Pennington and A. A. Martí, Unprecedented Dual Light-Switching Response of a Metal Dipyridophenazine Complex toward Amyloid-β Aggregation, *J. Am. Chem. Soc.*, 2016, **138**, 8686–8689.
46 A. Aliyan, T. J. Paul, B. Jiang, C. Pennington, G. Sharma, R. Prabhakar and A. A. Martí, Photochemical Identification of Molecular Binding Sites on the Surface of Amyloid-β Fibrillar Aggregates, *Chem*, 2017, **3**, 898–912.
47 V. Sathish, A. Ramdass, Z.-Z. Lu, M. Velayudham, P. Thanasekaran, K.-L. Lu and S. Rajagopal, Sensing of insulin fibrillation using alkoxy-bridged binuclear rhenium (I) complexes, *Inorg. Chem. Commun.*, 2016, **73**, 49–51.
48 M. T. Gabr and F. C. Pigge, Rhenium Complexes of Bis(benzothiazole)-Based Tetraarylethylenes as Selective Luminescent Probes for Amyloid Fibrils, *Chem. – Eur. J.*, 2018, **24**, 11729–11737.
49 A. S.-Y. Law, L. C.-C. Lee, M. C.-L. Yeung, K. K.-W. Lo and V. W.-W. Yam, Amyloid Protein-Induced Supramolecular Self-Assembly of Water-Soluble Platinum(II) Complexes: A Luminescence Assay for Amyloid Fibrillation Detection and Inhibitor Screening, *J. Am. Chem. Soc.*, 2019, **141**, 18570–18577.
50 K.-i. Watanabe, K. Nakamura, S. Akikusa, T. Okada, M. Kodaka, T. Konakahara and H. Okuno, Inhibitors of Fibril Formation and Cytotoxicity of β-Amyloid Peptide Composed of KLVFF Recognition Element and Flexible Hydrophilic Disrupting Element, *Biochem. Biophys. Res. Commun.*, 2002, **290**, 121–124.
51 J. L. Cifelli, T. S. Chung, H. Liu, P. Prangkio, M. Mayer and J. Yang, Benzothiazole Amphiphiles Ameliorate Amyloid β-Related Cell Toxicity and Oxidative Stress, *ACS Chem. Neurosci.*, 2016, **7**, 682–688.
52 Z. Yu, W. Guo, S. Patel, H.-J. Cho, L. Sun and L. M. Mirica, Amphiphilic stilbene derivatives attenuate the neurotoxicity of soluble Aβ42 oligomers by controlling their interactions with cell membranes, *Chem. Sci.*, 2022, **13**, 12818–12830.
53 S. Huo, J. Carroll and D. A. K. Vezzu, Design, Synthesis, and Applications of Highly Phosphorescent Cyclometalated Platinum Complexes, *Asian J. Org. Chem.*, 2015, **4**, 1210–1245.
54 J. Brooks, Y. Babayan, S. Lamansky, P. I. Djurovich, I. Tsyba, R. Bau and M. E. Thompson, Synthesis and Characterization of Phosphorescent Cyclometalated Platinum Complexes, *Inorg. Chem.*, 2002, **41**, 3055–3066.
55 J. Zhang, A. Sandberg, X. Wu, S. Nyström, M. Lindgren, P. Konradsson and P. Hammarström, trans-Stilbenoids with Extended Fluorescence Lifetimes for the Characterization of Amyloid Fibrils, *ACS Omega*, 2017, **2**, 4693–4704.
56 M. M. Hann, P. G. Sammes, P. D. Kennewell and J. B. Taylor, On double bond isosters of the peptide bond; an enkephalin analogue, *J. Chem. Soc., Chem. Commun.*, 1980, 234–235, DOI: **10.1039/C39800000234**.
57 D. P. Stockdale, J. A. Beutler and D. F. Wiemer, Synthesis of amide isosteres of schweinfurthin-based stilbenes, *Bioorg. Med. Chem.*, 2017, **25**, 5483–5489.
58 J. A. Suttil, J. F. Kucharyson, I. L. Escalante-Garcia, P. J. Cabrera, B. R. James, R. F. Savinell, M. S. Sanford and L. T. Thompson, Metal acetylacetonate complexes for high energy density non-aqueous redox flow batteries, *J. Mater. Chem. A*, 2015, **3**, 7929–7938.
59 J. Liu, C.-J. Yang, Q.-Y. Cao, M. Xu, J. Wang, H.-N. Peng, W.-F. Tan, X.-X. Lü and X.-C. Gao, Synthesis, crystallography, phosphorescence of platinum complexes coordinated with 2-phenylpyridine and a series of β-diketones, *Inorg. Chim. Acta*, 2009, **362**, 575–579.
60 P. L. Donabedian, T. K. Pham, D. G. Whitten and E. Y. Chi, Oligo(p-phenylene ethynylene) Electrolytes: A Novel Molecular Scaffold for Optical Tracking of Amyloids, *ACS Chem. Neurosci.*, 2015, **6**, 1526–1535.
61 L. Cui, S. Wang, J. Zhang, M. Wang, Y. Gao, L. Bai, H. Zhang, G. Ma and X. Ba, Effect of curcumin derivatives on hen egg white lysozyme amyloid fibrillation and their interaction study by spectroscopic methods, *Spectrochim. Acta, Part A*, 2019, **223**, 117365.
62 K. Pagano, S. Tomaselli, H. Molinari and L. Ragona, Natural Compounds as Inhibitors of Aβ Peptide Aggregation: Chemical Requirements and Molecular Mechanisms, *Front. Neurosci.*, 2020, **14**, 619667.
63 Á. Sarabia-Vallejo, P. López-Alvarado and J. C. Menéndez, Small-molecule theranostics in Alzheimer's disease, *Eur. J. Med. Chem.*, 2023, **255**, 115382.
64 J.-M. Suh, G. Kim, J. Kang and M. H. Lim, Strategies Employing Transition Metal Complexes To Modulate Amyloid-β Aggregation, *Inorg. Chem.*, 2019, **58**, 8–17.
65 A. I. Solomatina, A. D. Slobodina, E. V. Ryabova, O. I. Bolshakova, P. S. Chelushkin, S. V. Sarantseva and S. P. Tunik, Blood-Brain Barrier Penetrating Luminescent Conjugates Based on Cyclometalated Platinum(II) Complexes, *Bioconjugate Chem.*, 2020, **31**, 2628–2637.